Theoretical study of $Si^+(^2P_J)$-RG complexes and transport of $Si^+(^2P_J)$ in RG (RG = He – Ar)

William D. Tuttle[a], Rebecca L. Thorington[a], Larry A. Viehland[b*] and Timothy G. Wright[a**]

[a] School of Chemistry, University of Nottingham, University Park, Nottingham, NG7 2RD, UK

[b] Science Department, Chatham University, Pittsburgh, Pennsylvania, 15232, USA

* **Email**: Viehland@Chatham.edu

** **Email**: Tim.Wright@nottingham.ac.uk

Abstract

We calculate accurate interatomic potentials for the interaction of a singly-charged silicon cation with a rare gas atom of helium, neon or argon. We employ the RCCSD(T) method, and basis sets of quadruple-ζ and quintuple-ζ quality; each point is counterpoise corrected and extrapolated to the basis set limit. We consider the lowest electronic state of the silicon atomic cation, $Si^+(^2P)$, and calculate the interatomic potentials for the terms that arise from this: $^2\Pi$ and $^2\Sigma^+$. We additionally calculate the interatomic potentials for the respective spin-orbit levels, and examine the effect on the spectroscopic parameters; we also derive effective ionic radii for C^+ and Si^+. Finally, we employ each set of potentials to calculate transport coefficients, and compare these to available data for Si^+ in He.

1. Introduction

Silicon constitutes about 20% of meteoroids,[1] and upon entering the Earth's atmosphere, meteoric ablation occurs depositing atomic Si into the atmosphere. It is thought that the rapid reaction of Si with O_2 or O_3 precludes significant steady-state concentrations of Si and hence the usual means of forming atomic cations – charge transfer, thermal ionization and photoionization – are unlikely to be very important. Instead, the formation of SiO followed by charge transfer and subsequent reaction between SiO^+ and O leads to the production of Si^+ ions in the upper atmosphere.[2] Indeed, Si^+ is as abundant as Fe^+ and Mg^+ meteoric ions above 100 km, but its abundance decreases rapidly with altitude, such that very little is found below 95 km.[2] As such, the rapid depletion of Si^+ ions in the mesosphere and lower thermosphere has been of great interest in atmospheric chemistry - with various mechanisms proposed for the depletion[1,2,3] - and a good test of atmospheric models.[2] In that regard, in current models the relative injection rate of Si^+ into the upper atmosphere is larger than expected when compared to Fe^+ and Mg^+.[2]

Silicon ions are also present in the solar wind[4] and appear to play an important role in dense interstellar clouds, where ion-molecule reactions between Si^+ and H_2O are thought to be key in forming SiO,[5] which is predicted to take up more than 50% of the available silicon.[6] Additionally, although apparently not considered in the literature, cooling of Si^+ ions via interaction/complexation with prevalent He may be possible, in the same way as has been discussed with C^+ ions.[7,8] In passing, we note that fine structure excitation has been considered in the interaction of C^+ and Si^+ ^2P states with H atoms.[9]

Obtaining detailed kinetics for modelling the chemistry occurring in atmospheric or interstellar environments usually includes flow tube experiments, such as those carried out for Si^+.[10,11,12] As such, obtaining accurate ion mobility data for Si^+ in RG (RG = rare gas) is important for determining non-chemical loss mechanisms, as the flow gases are usually the light rare gases, i.e. RG = He–Ar. Mobilities also determine the relative energy of ions in flow tubes, and this is another incentive for obtaining such data. Besides, modelling plasmas such as in chemical vapour deposition (CVD), flames and other ion-molecule processes involving silicon[13,14] would benefit from such reliable data.

In the present work, we investigate the interatomic potentials that arise from $Si^+(^2P_J)$ interacting with $RG(^1S_0)$, where RG = He–Ar, and from these potentials we obtain accurate spectroscopic

constants and transport coefficients. First, we note that Si^+ has a ground electronic configuration of $1s^2 2s^2 2p^6 3s^2 3p^1$, which gives rise to a ^2P term; once spin-orbit (SO) coupling is considered, we have the $^2P_{3/2}$ and $^2P_{1/2}$ levels. In the absence of spin-orbit coupling, when Si^+ interacts with a closed-shell rare gas species, the ground ^2P atomic term evolves into a $^2\Pi$ and a $^2\Sigma^+$ diatomic term, with the former being the lower in energy. These terms have been investigated by previous theoretical workers; however, it is the SO-split $^2\Pi_\Omega$ and $^2\Sigma_\Omega{}^+$ levels which will be observed experimentally, and so we examine those here.

Under the influence of the spin-orbit interaction, the $Si^+(^2P)$ term splits into a higher $^2P_{3/2}$ and lower $^2P_{1/2}$ level, with a separation of 287.24 cm^{-1}.[15] In the Si^+-RG diatom, the $^2\Pi$ term also splits, resulting in a lower $^2\Pi_{1/2}$ level and a higher $^2\Pi_{3/2}$ level; in addition, the $^2\Sigma^+$ term becomes a $^2\Sigma_{1/2}{}^+$ level. The $^2\Pi_{1/2}$ level correlates with the lower $Si^+(^2P_{1/2})$ + RG($^1S_0$) asymptote while the $^2\Sigma_{1/2}{}^+$ and $^2\Pi_{3/2}$ levels both correlate with the higher $Si^+(^2P_{3/2})$ + RG($^1S_0$) asymptote. Furthermore, since Ω levels can interact if they have the same value, there is some mixing between the $^2\Pi_{1/2}$ and $^2\Sigma_{1/2}{}^+$ levels, but we retain the Russell-Saunders labels as this mixing is expected to be reasonably small; as such, the two levels will largely be dominated by a single ΛΣ state. It is also possible that further Ω mixing can occur, with diatomic SO levels arising from higher asymptotes, but the lowest excited Si^+ term (^4P) is over 40,000 cm^{-1} higher in energy, and such additional interactions are neglected here.

There have been several previous quantum chemical studies of the $Si^+(^2P)$-He(^1S) complex. Wong and Radom[16] reported the equilibrium internuclear separation, R_e, calculated at the MP3/6-311G(MC)** level (see ref. 16 for a description of the basis set), as part of an investigation of multiply-charged Si-He^{n+} species. Therein they also report the dissociation energy, D_0, at the MP4/6-311G(MC)(2d,2p) level, with a zero-point vibrational energy correction from their calculated harmonic vibrational frequency (obtained at the MP2/6-31G* level). In a follow-up study, Jemmis *et al.*[17] calculated R_e at both the MP2/6-31G* level and the QCISD(T)/6-311G(MC)** level.

Grice *et al.*[18] calculated counterpoise-corrected interaction potentials for both the $^2\Pi$ and $^2\Sigma^+$ terms of $Si^+(^2P)$-He(^1S), as well as the molecular terms arising from the $Si^+(^4P)$ + He(^1S) atomic asymptote. When employing the MP4SDTQ/6-311+G(3df,3pd) level of theory, they obtained the equilibrium internuclear separations and dissociation energies for these terms from interaction potentials. From these potentials they also computed the ion mobilities corresponding to each term, as well as the mobilities from the averaged transport cross sections,

where the terms were weighted by their degeneracies. Finally, Hughes and von Nagy-Felsobuki[19] optimised the geometry of the $^2\Pi$ state at the CCSD(T)_FC/cc-pVQZ level of theory, and computed the harmonic vibrational frequency at this level, with additional single-point energies utilising a range of Dunning-style basis sets to obtain dissociation energies.

As far as we are aware, there is no previous work on the $Si^+(^2P_J)$-$Ne(^1S_0)$ and $Si^+(^2P_J)$-$Ar(^1S_0)$ complexes.

With regard to ion mobility, there are experimental data for $Si^+(^2P_J)$ ions in helium from Fahey *et al.*[20] in 1981 who measured the ion mobility over the E/n_0 range 12 – 110 Td, where E is the electric field, n_0 is the gas number density and 1 Td = 10^{-21} V m^2. They worked at a temperature of 299 K and used two different pressures, 0.250 and 0.450 Torr; we will compare their values with our computed mobility data. In addition, there are calculated data for $Si^+(^2P_J)$ ions in He from ref.18, published in 1995, but no comparison to the earlier experimental values was made therein.

2. Computational methodology

2.1 Quantum chemistry

Interaction potentials with and without the SO interaction have been computed in the following manner for the diatomic levels which arise from the lowest atomic asymptotes of $Si^+(^2P_J)$ + $RG(^1S_0)$, with RG = He–Ar. Energies were computed at over 80 internuclear separations covering the equilibrium region, but also the short- and long-R separations (see Supplementary Material for actual R values employed). These separations were chosen so as to give converged ion transport properties for each species. The calculations were made at the RCCSD(T) level of theory as implemented in MOLPRO.[21] For all calculations, the 1s2s2p electrons of Si^+ were frozen; for Ne, the 1s electrons were frozen; and for Ar, the 1s2s2p electrons were frozen; all other electrons were correlated. Standard aug-cc-pwCVXZ (X=Q, 5) basis sets[22] were employed for Si^+, Ne and Ar, while aug-cc-pVXZ (X=Q, 5) basis sets[23] were used for He. The interaction energies at each internuclear separation were counterpoise-corrected (CP-corrected) to account for basis set superposition error (BSSE). The energies were computed with a high precision in MOLPRO, with energies converging to 10^{-12} E_h, orbitals in the SCF program to 10^{-8} E_h and the CCSD coefficients to 10^{-7} E_h. The T_1 diagnostic[24] values are below 0.04 in all cases, which suggests little multireference character; furthermore, the value is similar to our

previous work on $C^+(^2P_J)$-He($^1S_0$) and $C^+(^4P_J)$-He($^1S_0$),[25] where we noted good agreement with previously-reported multireference configuration interaction (MRCI) calculations.[26]

The CP-corrected interaction energies were used as the unperturbed eigenvalues of the Breit-Pauli SO matrix to allow calculation of RCCSD(T) interaction energies inclusive of SO splitting at each separation, as implemented in MOLPRO.[27] Subsequently, at each separation, a point-by-point extrapolation of each interaction energy to the basis set limit was performed using the two point (cubic) formula of Halkier *et al*.;[28,29] we denote the extrapolated potentials as RCCSD(T)/aV∞Z.

For each interaction potential, the rovibrational energy levels were obtained using the LEVEL program,[30] and the two lowest relevant levels were used in each case to obtain the spectroscopic constants from standard formulae, including the D_e value in the case of the vibrational anharmonicity constant. The isotopes employed in the spectroscopic parameter calculations were ^{28}Si, ^{4}He, ^{20}Ne and ^{40}Ar.

2.2 Transport coefficients

We calculated the transport cross sections for Si^+ in He, Ne and Ar from the *ab initio* interaction potentials as functions of the ion-neutral collision energy using the classical-mechanical program PC[31] that is an improved version of the earlier program QVALUES[32,33]. We shifted each potential in energy by an amount that made the potential agree with the charge-induced dipole $1/R^4$ potential at 50 Å, with the largest shift only being 5.75×10^{-5} cm^{-1}. These shifts make no discernible difference to the calculated spectroscopic constants in Table 1, but improved the convergence of the transport properties.

The cross sections converged within 0.04% for He and Ne and within 0.03% for Ar, over wide ranges of collision energy. They were used in the program GC[32,34,35] to determine the standard mobility, K_0, and the other gaseous ion transport coefficients as functions of E/n_0 at gas temperatures of 100, 200, 300, 400 and 500 K, and also at 4.35 K in the case of RG = He. They were also used to compute the zero-field mobilities as a function of gas temperature. Calculations were performed for the specific isotope $^{28}Si^+$, while He, Ne and Ar were assumed to be the naturally occurring mixture of isotopes. The calculated mobilities are generally precise within the precision of the cross sections at E/n_0 values below 20 Td. The results are progressively less precise as E/n_0 increases to 1000 Td, but these details, as well as the mobilities and other transport properties, can be obtained from the tables placed in the database maintained from the University of Toulouse.[36] It should be noted that, if so desired, the

corresponding mobilities of other isotopes of Si^+ in each RG, or in mixtures thereof, can be determined from those of $^{28}Si^+$ using simple formulas.[37,38] These latter values are precise to four significant figures, which is comparable to doing the described calculations on the explicit systems.

3. Results and discussion

3.1 Spectroscopic Constants

Figure 1 shows the RCCSD(T)/aV∞Z interaction potentials for $Si^+(^2P_J)$-He, $Si^+(^2P_J)$-Ne and $Si^+(^2P_J)$-Ar. The interaction potentials for each SO level are shown, as well as those corresponding to the non-SO $^2\Pi$ and $^2\Sigma^+$ terms, which are the CP-corrected, basis-set extrapolated interaction energies, before the inclusion of the SO interaction. The data points required to plot these potentials are available as Supplementary Material. The spectroscopic constants obtained from these potentials are presented in Table 1, as are any previously reported values. We note that for all three complexes, $Si^+(^2P)$ with He–Ar, the $^2\Pi$ term is lower in energy than the $^2\Sigma^+$ term. A straightforward rationalization of this is that, for the $^2\Pi$ term, the unpaired Si^+ electron is in the $3p_x$ and $3p_y$ orbitals (which are perpendicular to the internuclear axis) whereas the $^2\Sigma^+$ term has the unpaired electron in the $3p_z$ orbital, which points along the internuclear axis. Hence, electron repulsion between the rare gas atom and the unpaired electron on Si^+ will be higher in the latter case.

For Si^+-RG, the $^2P_{3/2}$—$^2P_{1/2}$ SO splitting is calculated to be 257.3, 261.7 and 261.7 cm^{-1} for RG = He, Ne and Ar respectively. These are all in good agreement with the experimental value of 287.24 cm^{-1};[15] the differences can likely be attributed to interactions involving higher SO levels that were ignored here. The calculated SO splittings between the $^2\Pi_{1/2}$ and $^2\Pi_{3/2}$ levels at R_e were found to be 186.7, 183.5 and 178.0 cm^{-1} for RG = He–Ar respectively, which suggests that these systems can be reasonably well described by Hund's case (a) coupling, since the asymptotic ^2P_J splitting is approximately 3/2 times the molecular $^2\Pi_\Omega$ splitting.[39]

3.1.1 $Si^+(^2P_J)$ with helium

The RCCSD(T)/aV∞Z interaction potentials for the $Si^+(^2P_J)$-He($^1S_0$) levels are given in Figure 1(a). From Table 1, it can be see that the $^2\Pi_{3/2}$ level has spectroscopic constants almost identical to the non-SO $^2\Pi$ term, which is expected as there is no other $\Omega = 3/2$ level with which the former can interact. The $^2\Pi_{1/2}$ level can interact with the $^2\Sigma_{1/2}{}^+$ level (both $\Omega = ½$); this occurs to differing extents with all three rare gas species studied here, but the mixing is strongest for helium, where the $Si^+(^2P_J)$ spin-orbit splitting is of the same magnitude as the $^2\Pi$ well depth.

The dissociation energy, D_e, is reduced by almost 30% for the $^2\Pi_{1/2}$ level compared to the $^2\Pi$ non-SO term, and the harmonic vibrational frequency, ω_e, and force constant, k, also decrease, by 13% and 25% respectively. These same measures increase for the $^2\Sigma_{1/2}^+$ level compared to the $^2\Sigma^+$ term, with D_e increased by 30%, ω_e increasing by 23% and k by 50%. The perturbations are larger for the $^2\Sigma_{1/2}^+$ level than for the $^2\Pi_{1/2}$ level as the two potentials are closer energetically near the $^2\Sigma^+$ equilibrium internuclear separation, and so more mixing occurs here than near the $^2\Pi$ term minimum; this mixing gives more bonding character to the $^2\Sigma_{1/2}^+$ level and, concomitantly, a reduction in bonding for the $^2\Pi_{1/2}$ level. Similar observations were made for $C^+(^2P_J)$-$He(^1S_0)$,[25] but the SO splitting for $C^+(^2P_J)$ is only 63.42 cm^{-1},[40] so the mixing between the SO levels was significantly weaker, with only a 4% reduction in D_e for the $^2\Pi_{1/2}$ level compared to the $^2\Pi$ term, while the reductions in ω_e and k were less than 1% (again with the changes being more significant for the $^2\Sigma_{1/2}^+$ level).

In Figure 2, we show the SO interaction potentials which all approach an asymptotic value of zero at long internuclear separations. As well as being more useful for the transport coefficient calculations (with minor shifts, as noted above), the interaction potentials allow changes in well depth and well shape to be more evident. The offset curves are shown in Figure 2(a) for $Si^+(^2P_J)$-$He(^1S_0)$. For both the $^2\Pi_{1/2}$ and the $^2\Sigma_{1/2}^+$ levels, the anharmonicity constant, $\omega_e x_e$, increases compared to the non-SO (unmixed) potentials, by 25% for the former level and by 17% for the latter; this indicates a differential mixing effect with R and so a change in the shape of the potential. Additionally, the equilibrium rotational constant, B_e, which was not very sensitive to the Ω-mixing in $C^+(^2P_J)$-$He(^1S_0)$[25] (and as will be shown below is not particularly sensitive to mixing in the Si^+-Ne and Si^+-Ar cases) decreases by 2% for the $^2\Pi_{1/2}$ level and increases by almost 9% for the $^2\Sigma_{1/2}^+$ level compared to the non-SO terms; these changes in the rotational parameters also indicate changes to the shapes of the potentials arising from Ω-mixing.

Although there is no previous work computing interaction potentials or equilibrium geometries of the SO levels, we are able to compare to previous calculations on the non-SO $^2\Pi$ and $^2\Sigma^+$ terms. The equilibrium geometry for the $^2\Pi$ term obtained by Wong and Radom[16] at the MP3/6-311G(MC)** level is almost 0.5 Å longer than that obtained in the current work, with the D_e value obtained from their structure at the MP4/6-311G(MC) (2d,2p) level being only ~84 cm^{-1}, significantly lower than the 246.1 cm^{-1} value obtained here. Jemmis *et al.*[17] obtained an R_e value of 3.227 Å at the QCISD(T)/6-311G(MC)** level, which is surprisingly longer than the value obtained here of 2.769 Å. We note also that in that work, at the same level of

theory, a value for the equilibrium bond length of the $^2\Pi$ term was obtained for $C^+(^2P)$-He that was 0.3 Å longer than that in our previous RCCSD(T)/aV∞Z interaction potential study.[25]

Grice *et al.*[18] obtained BSSE-corrected interaction potentials at the MP4SDTQ/6-311+G(3df,3pd) level of theory for both the $^2\Pi$ and $^2\Sigma^+$ terms, and from these found equilibrium internuclear separations of 2.94 Å for the $^2\Pi$ term and 3.95 Å for the $^2\Sigma^+$ term. The BSSE correction was performed with the full (we assume) counterpoise correction, but the values presented in Table 1 of that work are a little ambiguous: the relevant columns are labelled "without BSSE" and "incl. BSSE", and at first glance it is not clear whether this is as stated or whether it is meant to imply "without BSSE correction" and "incl. BSSE correction". Since the "incl. BSSE" D_e value is lower than the "without BSSE" one, we take the column headings to mean "without BSSE correction" and "including BSSE correction". Their R_e values are both in reasonably good agreement with those obtained in the present work, although interestingly the slightly shorter equilibrium geometries from the interaction potentials without correcting for BSSE are in better agreement with the present values. D_e values were also obtained from the interaction potentials, with overall a reasonable agreement with the present D_e values; the $^2\Sigma^+$ term D_e value from the BSSE-corrected potentials is in excellent agreement with the present work, while for the $^2\Pi$ term the potentials without BSSE correction yielded a value in better agreement with the current study.

Finally, Hughes and von Nagy-Felsobuki[19] reported a CCSD(T)_FC/cc-pVQZ equilibrium structure of 2.799 Å for the $^2\Pi$ term, in very good agreement with the value obtained here. In reference 19 this is compared to a value of 2.437 Å obtained by Jemmis *et al.*[17], but this appears to be a misquoted value of R_e for the $^1\Sigma^+$ term of Si^{2+}-He, and the value for the $^2\Pi$ term of Si^+-He from reference 17 is actually 3.227 Å. We note that Hughes and von Nagy-Felsobuki also obtained dissociation energies with both aug-cc-pVTZ and cc-pVQZ basis sets, with the former giving a D_0 value of 276 cm^{-1} and the latter 251 cm^{-1}. Comparing to the value of 193.3 cm^{-1} obtained here, it is obvious that the cc-pVQZ basis set gives a slightly better agreement, in contrast to C^+-He, where the aug-cc-pVTZ value was closer to our previously obtained value,[25] presumably due to the importance of diffuse functions. A value of ω_e was also obtained in reference 19, and it is in very good agreement with the value found here. As such it seems possible that the poor dissociation energy calculated with the cc-pVQZ basis set is due to lack of diffuse functions, while the poorer agreement with aug-cc-pVTZ is a more general basis set size issue.

In summary, although various methods and basis sets have been used to calculate the more-common spectroscopic parameters for Si^+-He, all apparently suffer from the level of inclusion of electron correlation energy, the basis set quality, or both. No previous study has considered the spin-orbit potential energy curves.

3.1.2 $Si^+(^2P_J)$ with neon and argon

Figures 1(b) and 1(c) show the interaction potentials for $Si^+(^2P_J)$-Ne($^1S_0$) and $Si^+(^2P_J)$-Ar($^1S_0$), shifted the match the respective calculated spin-orbit asymptotic energies. Figures 2(b) and 2(c) show the interaction potentials each approaching an asymptotic value of zero to make clear any changes to the shapes and depths of the SO potentials as a result of Ω-mixing. As for $Si^+(^2P_J)$-He($^1S_0$), the $^2\Pi_{3/2}$ level has no other Ω=3/2 levels with which it can interact in this three-state picture, and so the spectroscopic constants are effectively identical to those of the non-SO $^2\Pi$ term; this can be seen from the coincidence of the $^2\Pi$ and $^2\Pi_{3/2}$ potentials in Figures 2(b) and 2(c) for RG = Ne and Ar respectively. Also, as for $Si^+(^2P_J)$-He($^1S_0$), the $^2\Pi_{1/2}$ level can interact with the $^2\Sigma_{1/2}{}^+$ level, but as the rare gas changes from helium to neon to argon, the energetic separation between the $^2\Sigma^+$ and $^2\Pi$ term interaction potentials increases, reducing the extent of the mixing of the two states. This is apparent both upon visual inspection of the potentials and from the spectroscopic constants; for $Si^+(^2P_J)$-RG($^1S_0$), the $^2\Pi_{1/2}$ level D_e value decreases by around 15% (versus the non-SO $^2\Pi$ term) for neon and only 3% for argon, whereas for helium this was almost 30%. Similarly, the reductions in ω_e and k are smaller for the higher atomic number rare gas species; ω_e decreases by 3% while k decreases by 6% for neon and both decrease by under 1% for argon. These changes are mirrored in the values of D_e, ω_e and k for the $^2\Sigma_{1/2}{}^+$ level compared to the non-SO $^2\Sigma^+$ term, with a 26% increase in D_e for neon and a 15% increase for argon (versus a 30% increase for helium). As noted above for the helium complex, the $^2\Sigma^+$ term is more strongly affected by the mixing when forming the SO levels than the $^2\Pi$ term as it is energetically closer to the $^2\Pi$ term at its equilibrium internuclear separation, and even though the separation between the two terms is increasing down the rare gas series, this overall picture still applies.

Whereas significant changes in B_e and $\omega_e x_e$ were observed in the $^2\Pi_{1/2}$ and $^2\Sigma_{1/2}{}^+$ levels (compared to the non-SO terms) for RG = He, attributable to the changing shape of the potentials from R-dependent Ω-mixing, this becomes much less apparent down the group, especially for the $^2\Pi_{1/2}$ level. For the neon complex B_e decreases by under 1% and $\omega_e x_e$ increases by 14% (versus 25% for helium), while for the argon complex both values change by

less than 1%. Since the $^2\Pi$ well depth for the argon complex is over 5 times that of the neon complex, the shape of that potential is almost unaffected by the Ω-mixing. For the $^2\Sigma_{1/2}{}^+$ level, B_e increases by 6% for the neon complex and about 2% for the argon complex relative to the non-SO term, while $\omega_e x_e$ increases by 19% for the neon complex and decreases by 5% for the argon complex.

Comparing the complexes, we see the expected increase of binding energy with increasing polarizability of the RG atom for both the $^2\Pi$ and $^2\Sigma^+$ states and their SO components. It is interesting to note a decrease in R_e with atomic number of the RG atom for the $^2\Pi$ SO and non-SO states and this indicates that the attractive forces are increasing (via the polarizability) faster than the repulsive ones (mainly arising from electron repulsion). On the other hand, the trend is not monotonic for the $^2\Sigma^+$ states, with a decrease from Si^+-He to Si^+-Ne, and then an increase from Si^+-Ne to Si^+-Ar. This suggests a subtler balance between the attractive and repulsive terms, with the increase in the latter being comparable to the former, likely as a result of the unpaired electron now being located along the internuclear axis (in contrast to the $^2\Pi$ state).

We can also compare results for Si^+-He with those of C^+-He in our previous work.[25] Concentrating on the non-SO results, we see R_e values of 2.200 Å and 2.968 Å for the $^2\Pi$ and $^2\Sigma^+$ states of C^+-He, both considerably smaller than those of Si^+-He (Table 1), and corresponding D_e values of 476.1 and 121.8 cm^{-1}, both considerably higher than those for Si^+-He. The R_e values can simply be explained by the expected smaller ionic radius of C^+ compared to Si^+ (see below). The D_e result can be explained similarly since the He atom can approach the C^+ closer than it can for Si^+ and this increases the magnitude of the attractive terms; concomitantly, there are fewer electrons on C^+ to contribute to the repulsive terms.

Finally, we note that we can derive Wright-Breckenridge ionic radii, R^{WB}, of C^+ and Si^+ from the calculated R_e values of C^+-He and Si^+-He, respectively, by simply subtracting 1.49 Å.[41] This yields values of 0.71 Å and 1.28 Å when considering the (non-SO) $^2\Pi$ state, and 1.48 Å and 2.37 Å, when considering the (non-SO) $^2\Sigma^+$ state. The latter two values are roughly twice the size of the former and indicate the effect of approaching the cation from different directions when there is an unpaired electron. An estimate of the Pauling radius for C^+ is 0.29 Å and for Si^+ is 0.65 Å,[42] both considerably smaller than those derived herein; however, these must be based on hypothetical or interpolated/extrapolated results since these ions do not form ionic compounds naturally. (In ref. 41 it was found that R^{WB} agreed well with other values when the cation formed part of actual ionic compounds, but poorly in other cases.)

3.2 Transport coefficients

Ion mobilities, diffusion coefficients and other transport coefficients have been calculated from the SO interaction potentials arising from the lowest doublet levels of Si^+ interacting with the rare gases helium, neon and argon. The weightings chosen to calculate the ion mobilities were those of the ground state (100% $^2\Pi_{1/2}$ cross-sections), the excited state (a 1:1 weighting of the $^2\Pi_{3/2}$ and $^2\Sigma_{1/2}^+$ cross-sections) and a statistical state (a 1:1:1 weighting of $^2\Pi_{1/2}$, $^2\Pi_{3/2}$ and $^2\Sigma_{1/2}^+$ cross-sections). Since experimental ion mobility values are only available for Si^+ in He, we only compare those to experiment here, but we also show the mobilities for Si^+ in Ne and Ar. The full dataset of calculated ion transport properties is available in the Toulouse database.[36]

In Figure 3(a) are plotted the experimental Si^+ in He mobility results from Fahey et al.[20] with error bars that they estimated as 5 %. In those experiments, the Si^+ ions were formed via electron impact on $Si(CH_3)_4$ followed by mass selection prior to injection into the drift tube. This can lead to an unknown mixture of levels/states (particularly the spin-orbit ones of concern here), incomplete translational thermalization of the ions, and injection effects as the ions are steered into the drift tube (a particular problem with low-mass He as the buffer gas).

There are some immediate remarks to be made about Figure 3(a). First, it is notable that the experimental data fall between the calculated mobilities of the two individual ^2P_J states. Further, even the mobilities that were calculated assuming a statistical mix of the atomic spin-orbit states are barely within the error bars; these latter values are, however, in much better agreement than the individual spin-orbit states.

There is clearly some residual disagreement between the calculated statistical mobilities and the experimental results; moreover, this seems to be largely constant across the E/n_0 range. Therefore, it is likely that thermalization of the Si^+ ^2P_J spin-orbit states has occurred in the ion source for the mobility measurements. The first obvious explanation for the remaining disagreement is simply that the estimated error bars should in fact be larger than assumed. Another possibility is that there are residual systematic errors and this might be associated with the ion injection process. There are two aspects to this: the deceleration of the Si^+ ions via collisions with He; and non-uniform field effects caused by the injection ion optics. Both of these effects can have an influence on the effective length of the drift tube experienced by the ions, and hence on the overall calculated mobility. It would be interesting to repeat these measurements on a well-defined apparatus and also to investigate the effects of varying the injection voltage and buffer gas.

At this point we mention that Grice et al.[18] also calculated mobilities in their work, employing their MP4(SDTQ)/6-311+G(3df,3pd) potentials. This level of theory should be sufficient to produce reasonably reliable potential energy curves, but Table 1 indicates that in fact their R_e value is 0.17 Å too long (comparing with our non-SO $^2\Pi$ value), even after correction for BSSE. Further, their calculated dissociation energy, D_e, is 62 cm^{-1} lower than the present value, which is a significant percentage difference. As they note in their work, different D_e values can affect the calculated mobilities significantly, which is why they investigated the effect of BSSE in that work. That their BSSE-corrected values are still in poor agreement with those here suggests that the level of calculation they employed is not sufficient for this system. It is not surprising, therefore, that the calculated mobilities in ref. 18 are not in good agreement with those obtained in the present work, nor those measured in ref. 20 – see Figure 3(a).

In addition to the weaknesses in the potentials employed by Grice et al.,[18] there are also deficiencies in their calculated mobilities. First, it is not clear at what temperature the mobilities were calculated (in making the comparisons herein we are assuming this was 300 K). Secondly, their calculated method were obtained by using the three-temperature (3T) theory,[43,44] rather than the Gram-Charlier approach[34,35] used in the present work. Finally, other calculated values in the same paper, such as Na^+ in He, are not in good agreement with experiment.[45] In conclusion, the present comparison of the calculated results of ref. 18 with those in the present work and the experimental results of ref. 20, indicate that the calculated ones in ref. 18 should be treated with caution; this likely also applies to their mobilities for $Si^+(^4P)$.

We now consider all three plots in Figure 3. First we note that there is the expected lowering of mobility overall as the buffer gas becomes heavier, which of course feeds through to the zero-field mobilities. Secondly, there is the expected better-defined maximum in the mobility variation with E/n_0 as the buffer gas becomes heavier. We also note the appearance of a small mobility minimum for Si^+ in Ar for the $^2P_{1/2}$ curve, which is an indication that attractive terms beyond the ion-induced dipole interaction are important near the potential minimum.

Another interesting observation is that there is a reversal in the ordering of the zero-field mobilities for the $^2P_{1/2}$ and $^2P_{3/2}$ levels as we move from He to Ar. On the other hand the ordering at high E/n_0 remains the same, with the maxima also being in the same order. These maxima are located below 10 K for Si^+ in He and Ne, but in Ar they are at 3700 K for $^2P_{3/2}$, 7600 K for $^2P_{1/2}$ and 5300 K for the statistical case. These stark differences between the systems

may be rationalized by the mobilities being dominated by the long-range potential in the case of Ar, but by the minimum and repulsive wall regions in the cases of He and Ne.

4. Concluding remarks

In conclusion, we have calculated reliable interatomic potentials for Si^+ interacting with each of He, Ne and Ar. The level of theory and extrapolation of already-large basis set results to the basis set limit, along with correction for BSSE, support the assertion of reliability; the inclusion of spin-orbit coupling has been made for the first time for these systems and this also will allow a more direct comparison with experimental spectroscopic and (further) mobility data when they become available. Using the potentials, we have calculated values for various spectroscopic parameters. Trends for the Si^+-RG parameters have been discussed and comparisons between Si^+-He and C^+-He were made. In addition, we have estimated the ionic radii of Si^+ and C^+; in both cases different effective radii result depending on the approach direction of He with respect to the unpaired electron

Another assessment of reliability would be with experimental ion mobilities, but unfortunately there only appears to be one set of data available for Si^+ in He and none for the other two systems. On top of the estimated experimental uncertainty of 5%, the indications are that there may be a systematic error present in the experimental mobility results for Si^+ in He[20] and so clearly other measurements would be useful.

The provision of reliable spectroscopic data is important since silicon ions are prevalent in many chemical applications as well as in the Earth's atmosphere (and likely that of other planets). Additionally, Si^+ is present in the interstellar medium. As a consequence, reliable modelling of such systems requires accurate experimental rate coefficients and in turn these often require atomic ion loss mechanisms to be taken into account. Chemical models can also make use of knowledge of molecular energy levels via statistical thermodynamics and master equation approaches to calculate thermodynamic and kinetic data. To this end we have included the vibrational energy levels in the Supplementary Information, which can be used in tandem with the rotational constants and separations of the Si^+-RG spin-orbit levels to generate standard thermodynamic quantities and their variation with temperature and pressure. Although further improvements in calculation can be made, it is doubtful that they will impact greatly on the lower energy (thermally-populated) levels; hence thermodynamic and kinetic data should be reliable using the present data. We do note, however, that any interest in the

near-dissociation energy levels would require an improvement even over the very high-level results reported herein.

Acknowledgements

T. G. Wright, W. D. Tuttle and R. L. Thorington are grateful for the provision of computational time by the Engineering and Physical Sciences Research Council (EPSRC) under the auspices of the National Service for Computational Chemistry Software (NSCCS), and are also grateful for access to the University of Nottingham High Performance Computing Facility. The EPSRC and the University of Nottingham are thanked for the provision of a studentship to W. D. Tuttle.

Figure Captions

Figure 1. Interaction potentials for (a) $Si^+(^2P_J)$-$He(^1S_0)$, (b) $Si^+(^2P_J)$-$Ne(^1S_0)$ and (c) $Si^+(^2P_J)$-$Ar(^1S_0)$, each curve relative to its respective calculated spin-orbit asymptotic energy. The dashed lines show the non-SO potentials, while the solid lines with markers show the SO potentials. Note that although these are interaction potentials, they have been shifted so that zero energy is defined as the non-SO asymptote.

Figure 2. Interaction potentials for (a) $Si^+(^2P_J)$-$He(^1S_0)$, (b) $Si^+(^2P_J)$-$Ne(^1S_0)$ and (c) $Si^+(^2P_J)$-$Ar(^1S_0)$, offset such that the each potential is degenerate at 50 Å matching the theoretical $1/R^4$ ion-induced dipole potential. The dashed lines show the non-SO potentials, while the solid lines with markers show the SO potentials. The $^2\Pi_{3/2}$ curve is essentially coincident with the $^2\Pi$ one and so cannot be seen.

Figure 3. Comparison of the experimental and calculated $^{28}Si^+(^2P_J)$ mobilities in helium at 300 K as a function of E/n_0 is shown in (a). The points with 5% error bars are the experimental values from Fahey *et al*.[20] The points without error bars are previously calculated values by Grice et al.,[18] which we have estimated from Figure 7 in that work. The calculated mobilities for $^{28}Si^+(^2P_J)$ in neon and argon are shown in (b) and (c), respectively. Note that these plots are semi-logarithmic.

Table 1. Spectroscopic constants for $^{28}Si^{+}(^{2}P_J)$-RG($^{1}S_0$) (RG = He – Ar)

State	R_e (Å)	D_e (cm^{-1})	D_0 (cm^{-1})	ω_e (cm^{-1})	$\omega_e x_e$ (cm^{-1})	k (N m^{1})	B_e (cm^{-1})	Reference
Si^{+}-He								
$^{2}\Pi_{1/2}$	2.803	175.3	131.0	97.3	17.36	1.954	0.613	This work
$^{2}\Pi_{3/2}$	2.769	246.2	193.4	112.5	13.93	2.613	0.628	This work
$^{2}\Pi$ (non-SO)	2.769	246.1	193.3	112.5	13.93	2.611	0.628	This work
	3.227	84		84				[a]
	3.227							[b]
	2.94	184						[c]
	2.799	329(304)	276(251)	107.0				[d]
$^{2}\Sigma_{1/2}^{+}$	3.703	60.1	38.4	49.5	11.93	0.506	0.351	This work
$^{2}\Sigma^{+}$ (non-SO)	3.861	46.2	28.5	40.4	10.19	0.336	0.323	This work
	3.95	42						[c]
Si^{+}-Ne								
$^{2}\Pi_{1/2}$	2.732	459.0	415.1	90.3	4.95	5.597	0.194	This work
$^{2}\Pi_{3/2}$	2.724	537.7	492.2	93.1	4.33	5.957	0.195	This work
$^{2}\Pi$ (non-SO)	2.724	537.6	492.2	93.1	4.33	5.956	0.195	This work
$^{2}\Sigma_{1/2}^{+}$	3.648	129.2	109.9	40.7	4.10	1.137	0.109	This work
$^{2}\Sigma^{+}$ (non-SO)	3.763	102.6	86.7	33.6	3.44	0.776	0.102	This work
Si^{+}-Ar								
$^{2}\Pi_{1/2}$	2.611	2685.8	2602.5	168.0	2.59	27.348	0.150	This work
$^{2}\Pi_{3/2}$	2.611	2769.6	2686.2	168.1	2.57	27.393	0.150	This work
$^{2}\Pi$ (non-SO)	2.611	2770.6	2687.1	168.1	2.57	27.403	0.150	This work
$^{2}\Sigma_{1/2}^{+}$	3.767	454.5	427.3	55.2	1.78	2.950	0.072	This work
$^{2}\Sigma^{+}$ (non-SO)	3.803	393.6	368.8	50.5	1.87	2.477	0.071	This work

[a] Wong and Radom[16] - MP3/6-311G(MC)** optimised structure with improved relative energies calculated using MP4/6-311G(MC)(2d,2p) on the MP3 structure. MP2/6-31G* harmonic frequencies used to obtain zero-point vibrational corrections, scaled by 0.93.

[b] Jemmis *et al.*[17] – QCISD(T)/6-311G(MC)** structure.

[c] Grice *et al.*[18] - MP4SDTQ/6-311+G(3df,3pd) BSSE corrected interaction potentials.

[d] Hughes and von Nagy-Felsobuki[19] - structure from CCSD(T)_FC/cc-pVQZ. D_e and D_0 obtained with the aug-cc-pVTZ (cc-pVQZ) basis sets; the D_e values have been obtained from the D_0 values using the cc-pVQZ ω_e value.

Figure 1.

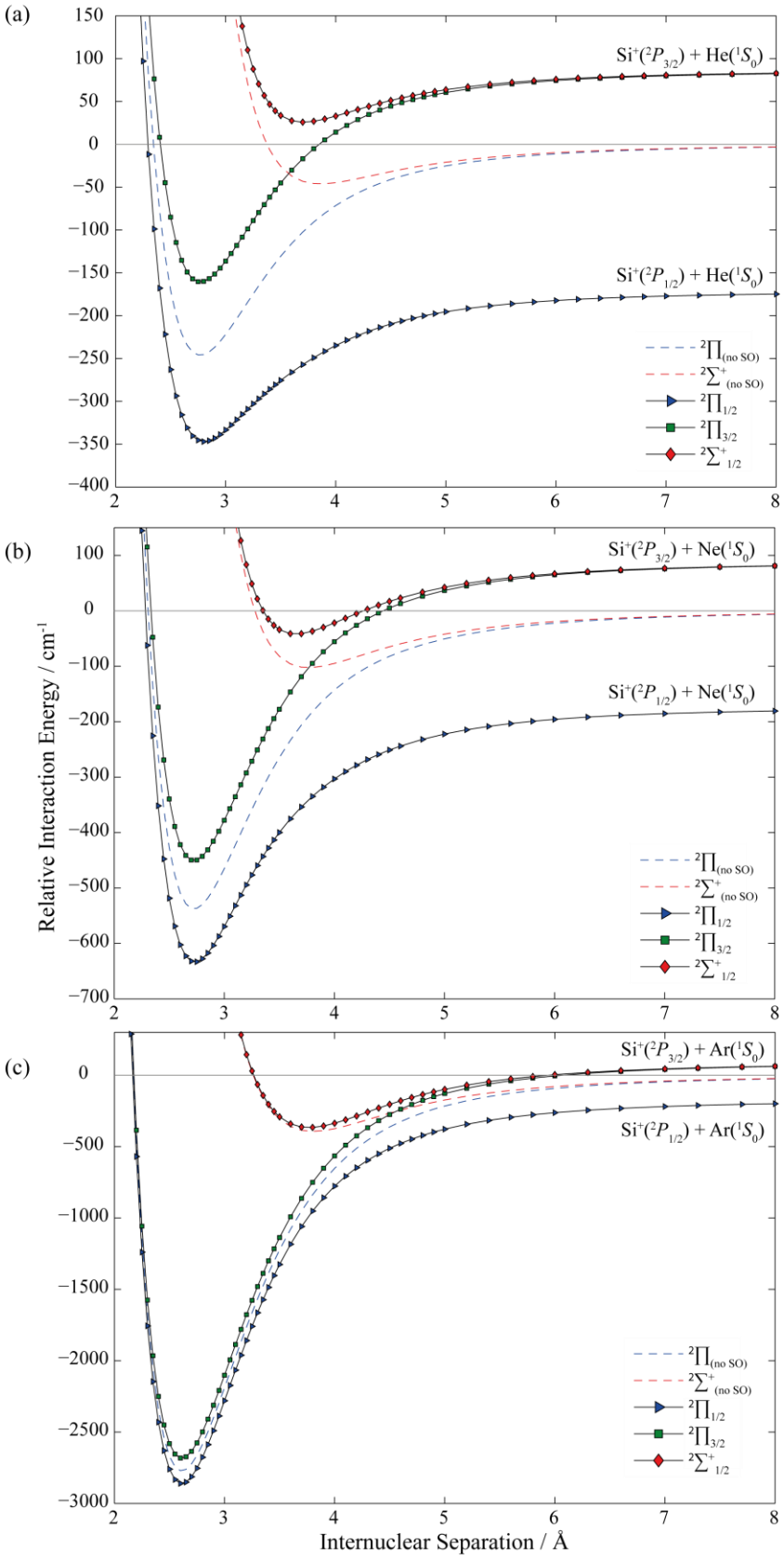
(a)
(b)
(c)
Si+(2P3/2) + He(1S0)
Si+(2P1/2) + He(1S0)
Si+(2P3/2) + Ne(1S0)
Si+(2P1/2) + Ne(1S0)
Si+(2P3/2) + Ar(1S0)
Si+(2P1/2) + Ar(1S0)
2Π(no SO)
2Σ+(no SO)
2Π1/2
2Π3/2
2Σ+1/2
Relative Interaction Energy / cm-1
Internuclear Separation / Å

Figure 2.

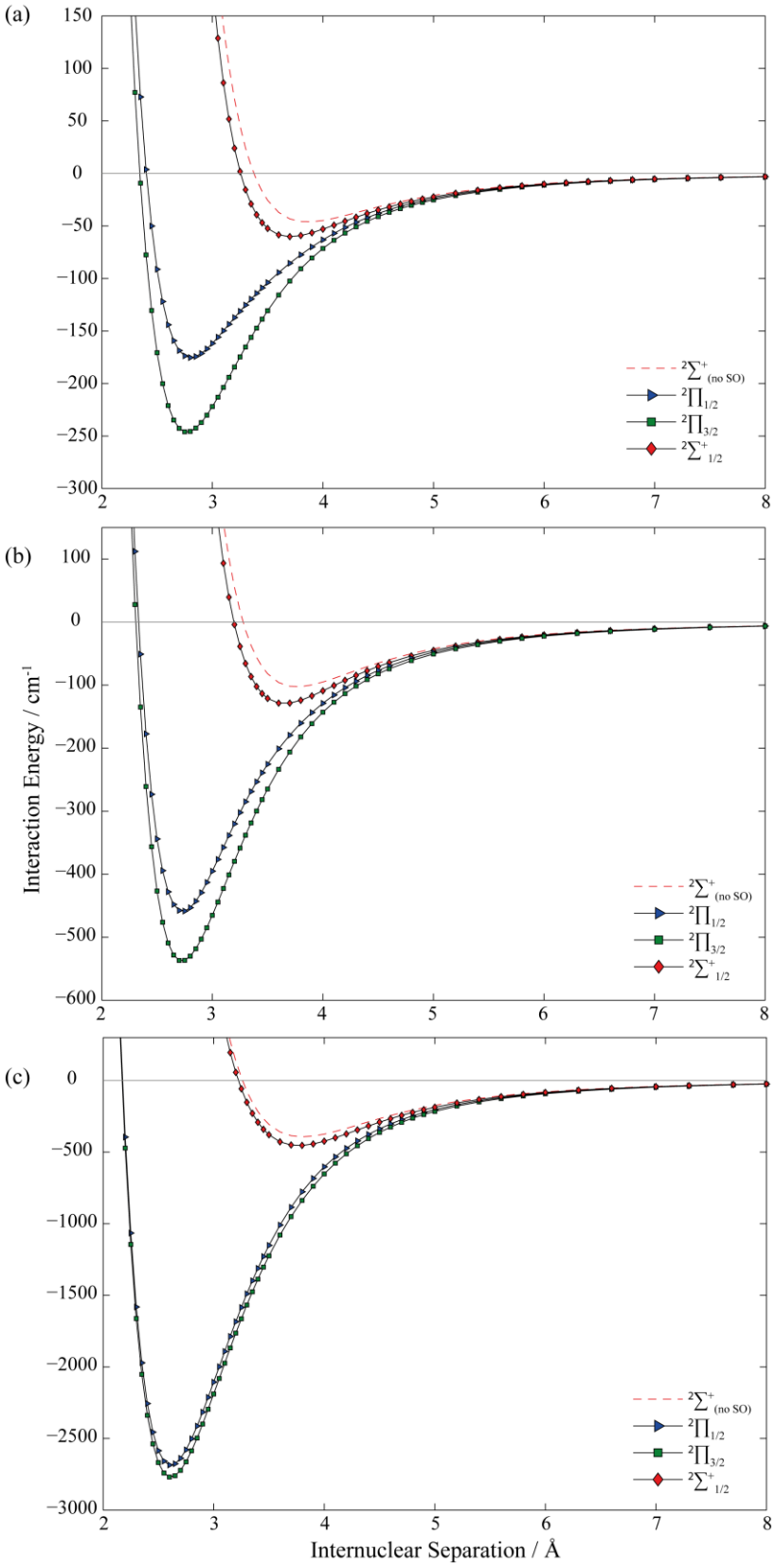
(a)
(b)
(c)
Interaction Energy / cm-1
Internuclear Separation / Å
2Σ+ (no SO)
2Π1/2
2Π3/2
2Σ+ 1/2

Figure 3.

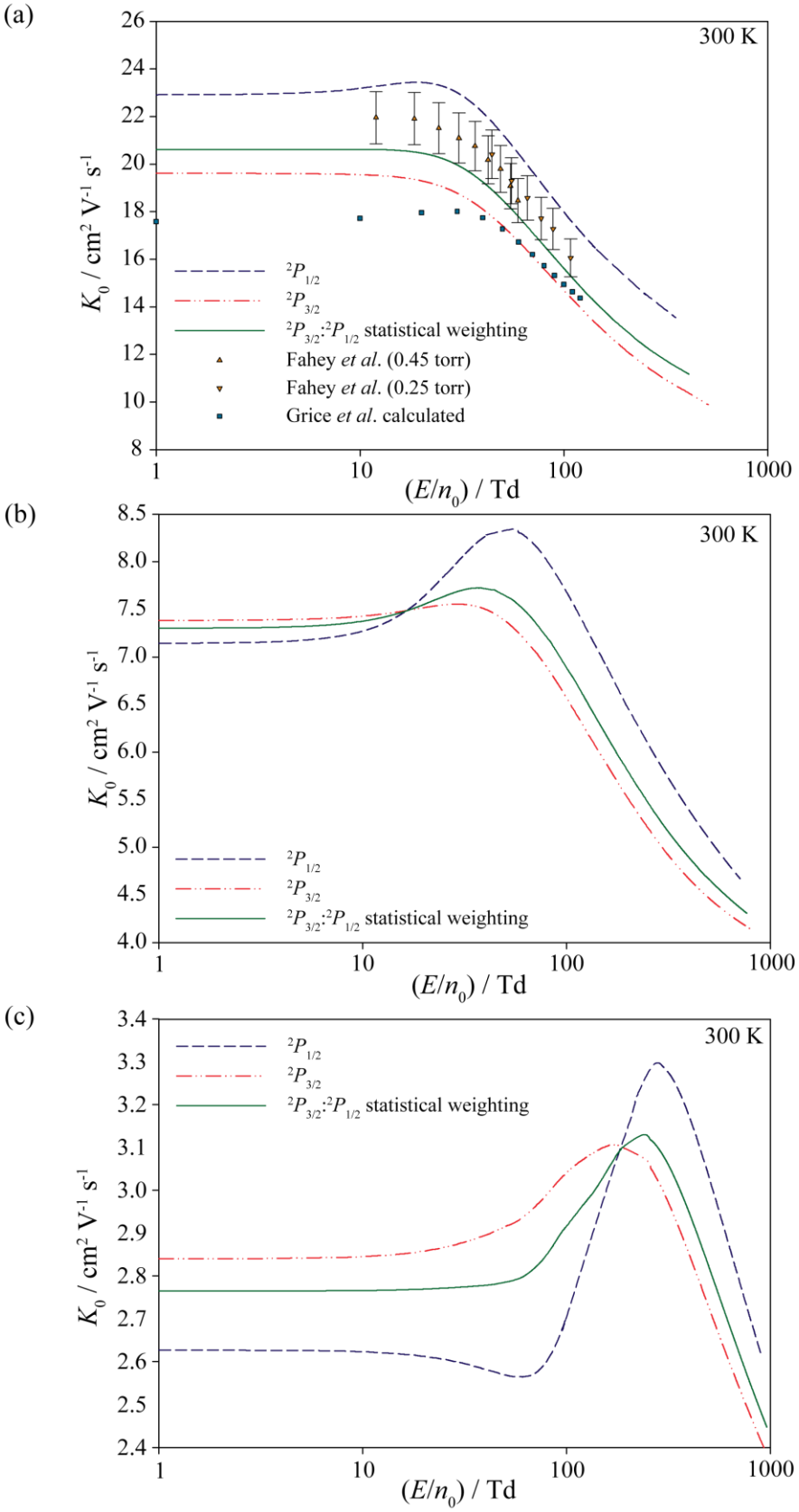
(a)
300 K
K_0 / cm^2 V^{-1} s^{-1}
(E/n_0) / Td
$^2P_{1/2}$
$^2P_{3/2}$
$^2P_{3/2}$:$^2P_{1/2}$ statistical weighting
Fahey et al. (0.45 torr)
Fahey et al. (0.25 torr)
Grice et al. calculated
(b)
300 K
K_0 / cm^2 V^{-1} s^{-1}
(E/n_0) / Td
$^2P_{1/2}$
$^2P_{3/2}$
$^2P_{3/2}$:$^2P_{1/2}$ statistical weighting
(c)
300 K
K_0 / cm^2 V^{-1} s^{-1}
(E/n_0) / Td
$^2P_{1/2}$
$^2P_{3/2}$
$^2P_{3/2}$:$^2P_{1/2}$ statistical weighting

References

[1] E. Kopp, F. Balsiger and E. Murad, Geophys. Res. Lett. **22**, 3473 (1995).

[2] J. M. C. Plane, J. C. Gómez-Martin, W. Feng and D. Janches, J. Geophys. Res. Atmos. **121**, 3718 (2016).

[3] E. E. Ferguson, D. W. Fahey, F. C. Fehsenfeld and D. L. Albritton, Planet. Space Sci. **29**, 307 (1981).

[4] P. Boschler, J. Geophys. Res. Space Physics, **94**, 2365 (1989).

[5] S. Wlodek, D. K. Bohme and E. Herbst, Mon. Not. R. Astron. Soc. **242**, 674 (1990).

[6] E. Herbst, T. J. Millar, S. Wlodek and D. K. Bohme, Astron. Astrophys. **222**, 205 (1989).

[7] S.W. Harrison, G.A. Henderson, L.J. Massa and P. Solomon, Astrophys. J. **189**, 605 (1974).

[8] N. Toshima, J. Phys. Soc. Jpn **38**, 1464 (1975).

[9] G. Barinovs, M. C. van Hemert, R. Krems and A. Dalgario, Astrophys. J., **620**, 537 (2005).

[10] J. C. Goméz-Martín, M. A. Blitz and J. M. C. Plane, Phys. Chem. Chem. Phys. **11**, 671 (2009).

[11] J. C. Goméz-Martín, M. A. Blitz and J. M. C. Plane, Phys. Chem. Chem. Phys. **11**, 10945 (2009).

[12] J. C. Goméz-Martín and J. M. C. Plane, Phys. Chem. Chem. Phys. **13**, 3764 (2011).

[13] J. H. Horton and J. M. Goodings, Can. J. Chem. **70**, 1069 (1992).

[14] *Ion–Molecule Reactions of Silicon Cations. Patai's Chemistry of Functional Groups.* S. Fornarini (Wiley Online, 1992). DOI: 10.1002/9780470682531.pat0252

[15] W. C. Martin and R. Zalubas, *J. Phys. Chem. Ref. Data.* **12**, 323 (1983).

[16] M. W. Wong and L. Radom, J. Am. Chem. Soc. **110**, 2375 (1988).

[17]E. D. Jemmis, M. W. Wong, H-B Bürgi and L. Radom, J. Molec. Struct. (Theochem) **261**, 385 (1992).

[18] S. T. Grice, P. W. Harland, R. G. A. R. Maclagan and A. E. Thompson, J. Chem. Soc. Faraday Trans. **91**, 4355 (1995).

[19] J. M. Hughes and E. I. von Nagy-Felsobuki, Eur. Phys. J. D **6**, 185 (1999).

[20] D. W. Fahey, F. C. Fehsenfeld, E. E. Ferguson and L. A. Viehland, J. Chem. Phys. **75**, 669 (1981).

[21] MOLPRO is a package of ab initio programs written by H.-J. Werner, P. J. Knowles, G. Knizia, F. R. Manby, M. Schütz, P. Celani, W. Györffy, D. Kats, T. Korona, R. Lindh, A. Mitrushenkov, G. Rauhut, K. R. Shamasundar, T. B. Adler, R. D. Amos, A. Bernhardsson, A. Berning, D. L. Cooper, M. J. O. Deegan, A. J. Dobbyn, F. Eckert, E. Goll, C. Hampel, A. Hesselmann, G. Hetzer, T. Hrenar, G. Jansen, C. Köppl, Y. Liu, A. W. Lloyd, R. A. Mata, A. J. May, S. J. McNicholas, W. Meyer, M. E. Mura, A. Nicklaß, D. P. O'Neill, P. Palmieri, D. Peng, K. Pflüger, R. Pitzer, M. Reiher, T. Shiozaki, H. Stoll, A. J. Stone, R. Tarroni, T. Thorsteinsson, M. Wang .

[22] N.B. Balabanov and K.A. Peterson, J. Chem. Phys. **123**, 064107 (2005).

[23] D.E. Woon and T.H. Dunning, Jr. J. Chem. Phys. **100**, 2975 (1994).

[24] T. J. Lee and P. R. Taylor, Int. J. Quant. Chem. S23 (1989) 199

[25] W. D. Tuttle, R. L. Thorington, L. A. Viehland and T. G. Wright, Mol. Phys. **113**, 3767 (2015).

[26] S. Matoba, H. Tanuma and K. Ohtsuki, J. Phys. B **41**, 145205 (2008).

[27] A. Berning, M. Schweizer, H.-J. Werner, P. J. Knowles and P. Palmieri, Mol. Phys. **98**, 1823 (2000).

[28] A. Halkier, T. Helgaker, P. Jorgensen, W. Klopper, H. Koch, J. Olsen and A. K. Wilson, Chem. Phys. Lett. **286**, 243 (1998).

[29] A. Halkier, T. Helgaker, P. Jorgensen, W. Klopper and J. Olsen, Chem. Phys. Lett. **302**, 437 (1999).

[30] R. J. LeRoy, *Level 8.0: A Computer Program for Solving the Radial Schrodinger Equation for Bound and Quasibound Levels*, University of Waterloo Chemical Physics Research Report CP-663, 2007.

[31] L. A. Viehland and Y. Chang, Comput. Phys. Comm. **181**, 1687 (2010).

[32] L. A. Viehland, Chem. Phys. **70**, 149 (1982).

[33] L. A. Viehland, Chem. Phys. **85**, 291 (1984).

[34] L. A. Viehland, Comput. Phys. Comm. **142**, 7 (2001).

[35] D. M. Danailov, L. A. Viehland, R. Johnsen, T. G. Wright and A. S. Dickinson, J. Chem. Phys. **128**, 134302 (2008).

[36] www.icecat.laplace.univ-tlse.fr

[37] L. A. Viehland, Int. J. Ion Mobility Spectrom. **19**, 1 (2016).

[38] L. A. Viehland, Int. J. Ion Mobility Spectrom. **19**, 11 (2016).

[39] D. Bellert and W. H. Breckenridge, Chem. Rev. **102**, 1595 (2002).

[40] C. E. Moore, *CRC Series in Evaluated Data in Atomic Physics* (CRC Press, Boca Raton, Fl, 1993), p. 339.

[41] T. G. Wright and W. H. Breckenridge, J. Phys. Chem. A **114**, 3182 (2010).

[42] Values found at https://www.webelements.com/periodicity/radius_ionic_pauling_1/ (accessed October 2016) which cites J.E. Huheey, E.A. Keiter, and R.L. Keiter in Inorganic Chemistry : Principles of Structure and Reactivity, 4th edition, HarperCollins, New York, USA, 1993, and J.E. Huheey, Inorganic Chemistry: Principles of structure and reactivity, 3rd edition, Harper International, New York, 1983, ISBN 0-06-042987-9.

[43] S. L. Lin, L. A. Viehland and E. A. Mason, Chem. Phys. **37**, 411 (1979).

[44] L. A. Viehland and S. L. Lin, Chem. Phys. **43**, 135 (1979).

[45] L. A. Viehland, J. Lozeille, P. Soldán, E. P. F. Lee and T. G. Wright, J. Chem. Phys. **119**, 3729 (2003).